Proceedings World Geothermal Congress 2026
Calgary, Canada, June 8 – 11, 2026

Stress, Slip, and Productivity: Integrated Geomechanical Modeling of the Þeistareykir Geothermal Reservoir – Part 1 Wellbore Scale

Irene C. Wallis[1]*, Drew L. Siler[2] and Anette Kærgaard Mortensen[3] and Guðjón Helgi Eggertsson[3]
Cubic Earth[1]*, Geologica Geothermal Group[2], and Landsvirkjun[3]
irene@cubicearth.nz

Keywords: Borehole image, permeability, drilling induced damage, stress, stress rotations, structural control

ABSTRACT

We present an innovative, multi-scale geomechanics analysis of Þeistareykir geothermal field, Iceland. Results were consistent across-scales and a good match to the distribution of reservoir productivity. Þeistareykir is a high temperature (~350°C), volcanic-hosted, two-phase geothermal system with 90 MWe of installed capacity. It is localized by an accommodation zone that consists of west-dipping normal faults to the north and east-dipping normal faults to the south. The wellbore-scale analysis, presented herein, focuses on integration of borehole image data to parameterize stress tensor models and reveal the wellbore-scale geologic controls on permeability. The reservoir-scale analysis, presented in a companion paper (Siler et al., 2026, this volume), focuses on static and dynamic geomechanical modelling of reservoir-scale faults.

Existing interpretations of eleven acoustic borehole image logs (ABI) were reviewed and three selected to constrain the stress tensor and explore controls on permeability through static geomechanical modelling. Detailed reinterpretation of drilling induced damage constrained the azimuth of horizontal stresses and revealed numerous stress rotations. These rotations matched the reservoir-scale dynamic modelling, providing cross-validation. Slip and dilatation tendency results were coherent with fracture characteristics, such as width, mineralization, and openness. First-order mechanical stratigraphy for all eleven wells provided an overall explanatory model for the distribution of feed zones and fracture frequency. Despite these insights, wellbore-scale analysis alone does not account for all feed zone locations and magnitudes. This highlights the central finding of this innovative multi-scale study: fluid flux into or out of a wellbore depends jointly on the features that are intersected and their connection to the reservoir-scale network of permeability.

1 INTRODUCTION

Þeistareykir is a high temperature (~350°C), basaltic-rift type volcanic-hosted geothermal system located in the Northern Rift Zone of Iceland. There is 90 MWe of installed capacity and around 8km^2 of drilled area. Like many of the Icelandic geothermal systems, Þeistareykir has relatively steep gradients in enthalpy, pressure, and permeability when compared to typical silicic rift or arc type volcanic-hosted geothermal systems (Wallis et al., 2023a). We undertook a novel, multi-scale geomechanical study to understand what controls the distribution of permeability at Þeistareykir (Figure 1).

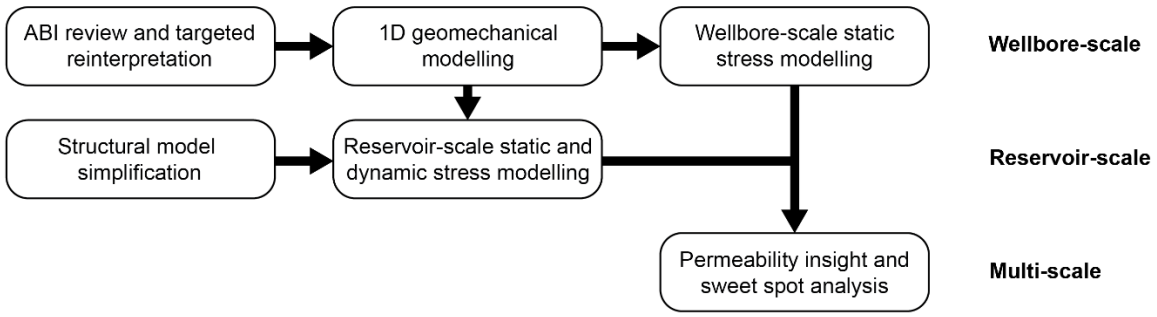


Figure 1. Workflow for the novel, multi-scale geomechanical study described herein and in the companion paper Siler et al. (2026 this volume).

In summary, our study seeks to define the geologic controls on permeability, with an emphasis on exploring the accumulation of favorable stress conditions that generate and maintain fault/fracture-hosted permeability. Static stress modelling involves calculation of fault or fracture slip and dilation tendency using the stress tensor defined by the geomechanical model(s) (Ferrill et al., 2020). Dynamic stress modelling calculates the change in

stress that results from failure on 3D faults (Siler, 2023), where a geomechanical model generalized from the wellbore-scale analysis defines a natural state. The results of stress modelling are compared with the distribution and magnitude of feed zones at the wellbore-scale and well capacity at the reservoir-scale. The wellbore-scale component of our study is described herein, while a companion paper addresses reservoir-scale (Siler et al., 2026, this volume).

2 DATA AND METHODOLOGY

Because acoustic borehole images (ABI) were acquired in almost all wells drilled between 2011 and 2023, there is a rich dataset with which to explore the wellbore-scale controls on permeability at Þeistareykir. These eleven acoustic borehole images were acquired by the Iceland GeoSurvey (ÍSOR) using the ABI-43 tool, a compact borehole imager that is temperature-rated to 170°C. The images were interpreted by either Iceland GeoSurvey (ÍSOR) or GeothermEx (GX), a Schlumberger company. These ABI data enable the identification of fractures that are open or partially open at the borehole wall using wave travel time (Wallis et al., 2023b). This contrasts with microresistivity borehole images (MBI) where we cannot easily determine if a fracture is open or not because electrically conductive fractures may either contain water or a conductive mineral (e.g., clay). However, the higher resolution and more complete picture of lithologic textures in an MBI image improves geologic feature type interpretation (e.g., differentiation between tectonic fractures and mechanical weaknesses parted by thermal stresses at the borehole wall), which means both technologies provide substantial value during subsurface characterization. All borehole images enable us to determine the attitude of fractures and azimuth drilling induced damage, which are central to this study where we investigate the controls on permeability using geomechanics.

2.1 Fracture Data

A total of 23,610 fractures had been identified in the eleven ABI. Fractures with complete or partial travel time anomalies are referred to here as ‘open’ (21%), acknowledging that a proportion of these will only be open at the borehole wall. Those without travel time anomalies are referred to as ‘closed’ (78%). Those where there is no classification based on travel time anomaly are referred to here as ‘unknown’ (1%). Due to their low probability of being tectonic in origin, the partial, lithobound fractures (N= 199) are excluded. When all data are considered, the mean fracture dip magnitude is 65 ± 20°, where closed fractures have a lower mean dip (64 ± 22°) than open (68 ± 18°, Figure 2). The NNE ↔ SSW strike trend dominates in the combined dataset, but there is local variation with mean fracture strikes trending N ↔ S or NE ↔ SW (Figure 3). Fractures with appreciable apertures have more clustered orientation trends than the entire fracture population (Figure 3). As expected, the fracture data interpreted from each ABI is impacted by borehole image quality and geometric sample bias, which is where fractures parallel or sub-parallel to the borehole are under sampled (Figure 3).

2.2 Drilling Induced Damage Data

Three ABI were selected for further analysis based on their location (they approximately span the wellfield), the overall quality of the ABI data, and their appropriateness for stress modelling. The latter is defined by (1) the presence of high confidence drilling induced damage and (2) an existing interpretation of fracture aperture/width.

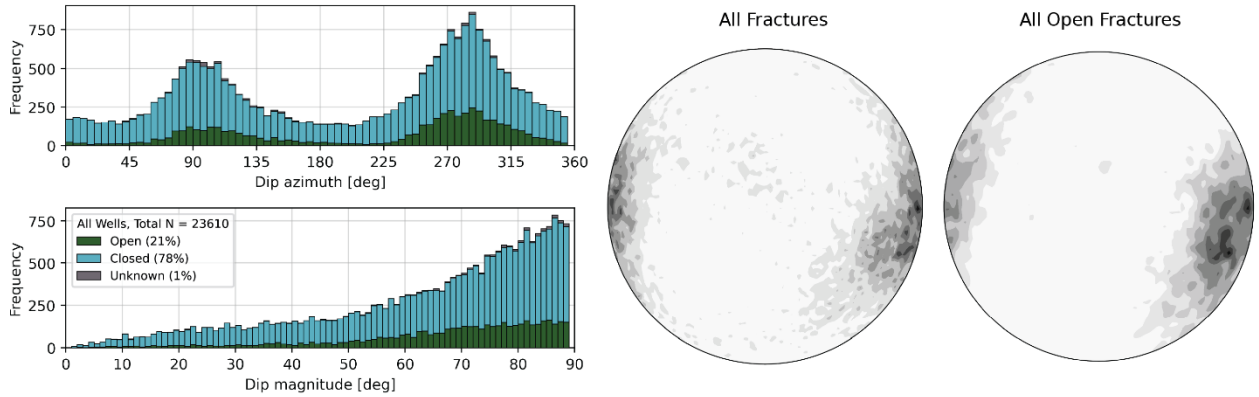


Figure 2: All fractures interpreted from ABI, classified as open, closed, and unknown using the method described in the text. Stereonets are equal area, lower hemisphere with Kamb contours of poles to plane.

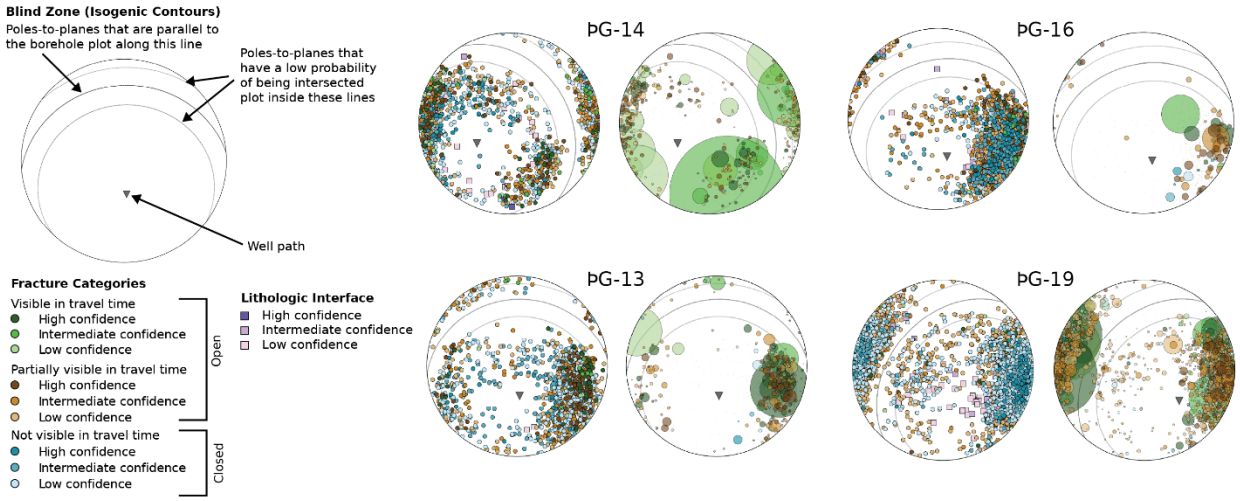


Figure 3: Illustration of how geometric sample bias impacts the distribution of fractures intersected by the well and, therefore, interpreted from the ABI. Poles to plane are plotted on lower-hemisphere, equal area stereonets with isogenic contours (Terzaghi, 1965; Fractoolbox, 2025). The same data is presented on two stereonets: one with fracture and lithology (interface) data plotted on the same scale (left stereonet for each well) and the other where markers are scaled by aperture/width (right stereonet for each well).

The selected wells were: (1) ÞG-14 (Árnadóttir et al., 2018), which is a relatively low temperature well on the northern edge of the drilled area with a high injectivity index (II); (2) ÞG-16 (Þorsteinsdóttir et al., 2018) which is a hotter well with a low II that is located on the western edge of the well field; and (3) ÞG-19 (Árnadóttir et al., 2024) which is hotter again, has a moderate II, and is located on the south-southwest side of the bore field (refer to Siler et al., 2026 this volume for a map of the bore field). We used the existing natural fracture interpretation in these wells, but conducted a more detailed interpretation of drilling induced damage. As well as identifying classic instances of borehole breakout (BHBO) and drilling induced tensile fractures (DITF), we also identified those DITF that interact with natural fractures (atypical DITF; Wallis et al., 2023b) and those BHBO that more resemble spalling at fracture intersections on the compressive sides of the borehole wall (atypical BHBO).

2.3 Lithologic Data and Mechanical Stratigraphy

Landsvirkjun provided a lithological interpretation of cuttings. We combined this with the ABI data to estimate the mechanical stratigraphy. Oversized intervals with low acoustic amplitude are interpreted to be softer formation than those intervals that were in-gauge and had a higher acoustic amplitude. Future advancement of this work would include integration of drilling parameters with the calculation of mechanical specific energy (Wyering et al., 2017) and petrophysical data where available.

2.4 1D Geomechanical Models

1D geomechanical models were constructed using methods described in Zoback (2010) and Peška and Zoback (1995), with geothermal-specific methodological adjustments as described in Wallis (2023). Pore pressure was constrained using a linear fit to the results of well pivot-point analysis that were provided by Landsvirkjun. The vertical stress was integrated using estimated mean rock properties and fluid density. Rock density and porosity was estimated using cuttings composition and local databases (Foged and Andreassen, 2016; Loftsson and Steingrímsson, 2010) because there are no petrophysical logs to surface to constrain this value. The Þeistareykir reservoir is two-phase and variation of steam quality greatly impacts fluid density. However, given the moderate to low porosities, the overall impact of this variation is low compared to the uncertainty associated with rock density. Subsequently, density for an approximately 50:50 mix of liquid and vapor was used (713 kg/m2). There are no extended leak-off tests at Þeistareykir to constrain the magnitude of the minimum stress (Wallis et al., 2020a), which is likely to be horizontal (S_{hmin}). Therefore, we must assume that the crust is in frictional equilibrium and use the Coulomb frictional-failure formulation with the limit on frictional failure defined by Byerlee (1978). The azimuth of the maximum horizontal stress (S_{Hmax}) was modelled using the method defined by Peška and Zoback (1995), and the mean azimuth of DITF. In their method, the magnitude of S_{Hmax} can be jointly inverted from drilling induced damage data providing the rock strength is known for BHBO or the tilt on DITF is well constrained. Neither is the case at Þeistareykir. The rock strength is greatly variable and could not be constrained reasonably using available data and the tilt of DITF is also greatly variable over short distances. Consequently, we developed a range of cases that covered simple normal ($S_{hmin} < S_{Hmax} < S_v$), transitional ($S_{hmin} < S_{Hmax} = S_v$), and strike slip ($S_{hmin} < S_v < S_{Hmax}$) conditions.

2.5 Slip and Dilatation Tendency

We calculated relative tendency of a fracture to undergo slip or dilatation given the magnitude and orientation of principal stresses (Ferrill et al., 2020). Slip tendency (T_s) is defined as:

Equation 1: $$T_s = \frac{\tau}{\sigma_n},$$

which is the ratio of shear (τ) and normal (σ_n) stress resolved on a fracture plane. Dilation tendency (T_d) is defined as:

Equation 2: $$T_d = \frac{(\sigma_1 - \sigma_n)}{(\sigma_1 - \sigma_3)},$$

where σ_1 is the maximum principal stress, σ_3 is the minimum principal stress, and σ_n is the normal stress resolved onto the fracture plane. We define hybrid tendency as:

Equation 3: $$T_h = T_s + T_d,$$

fractures with high hybrid tendency have an increased likelihood for permeability because shear plus dilation may generate volume or self-propping on asperities and/or fracture rugosity/sinuosity. These calculations do not account for the influence of rock strength on the likelihood that a fracture will self-prop, so we consider that separately using mechanical stratigraphy. If empirical rock strength data were available, future work could investigate the absolute value of fracture closure force (σ_n) against the ability of rock to withstand that force.

3 RESULTS

3.1 Drilling Induced Damage and Geomechanical Models

Geomechanical models were constructed to define the stresses for ÞG-14, ÞG-16, and ÞG-19, where the azimuth of S_{Hmax} was modelled from the mean DITF azimuth (Figure 4). The interpretation of drilling induced damage in ÞG-19 was limited by the generally poor image quality and the likely depths of stress rotation have been inferred to correspond with major lithologic transitions as indicated by the gamma and cuttings lithology (Figure 4, Features 7 and 8). Low confidence BHBO in ÞG -16 includes damage features that may be related to pipe wear on the low and high sides of the borehole, especially above 1700 mMD where their azimuths are rotated relative to DITF.

Abrupt rotations in azimuth of DITF were found in all cases, with two or three rotations in each well (Figure 4). Our S_{Hmax} modelling resulted in a 3- to 20-degree shift from the raw DITF azimuth. However, the stress rotations observed with depth persisted and, therefore, are not an artifact generated by changes in wellbore trajectory. Stress rotations are found to correspond with major faults, such as Feature 5 in ÞG-16 (Figure 4) where the rotation likely corresponds to a rift-edge fault that is mapped at surface. Stress rotations also correspond with feed zones (Figure 4), perhaps indicating the presence of other active faults that localize fluid flux. The depths of stress rotation in ÞG-19 were inferred from geologic data, so cannot be interpreted as correlating with the large feed zone with depth. However, we can say that this large feed zone does correspond with a transition from intermediate to basaltic rock compositions and a localized peak in fracture frequency that together may indicate the presence of a fault. Differences in S_{Hmax} azimuth between wells are discussed in a reservoir-scale companion paper (Siler et al., 2026, this volume).

3.2 Slip and Dilatation Tendency

Using the existing fracture interpretations for ÞG-14, ÞG-16, and ÞG-19 (Árnadóttir et al., 2018; Þorsteinsdóttir et al., 2018; Árnadóttir et al., 2024) and the geomechanical models described above, we calculated the slip (T_s), dilatation (T_d), and hybrid tendency (T_h) of each fracture. Results are presented here on a sail plots (Figure 5), where those fractures with highest T_h occur on the top right. S_{Hmax} azimuth rotations alter the range of T_s and T_d, so sail plots that aggregate all data from a well will be slightly offset. This is most clearly seen in ÞG-14 and ÞG-19.

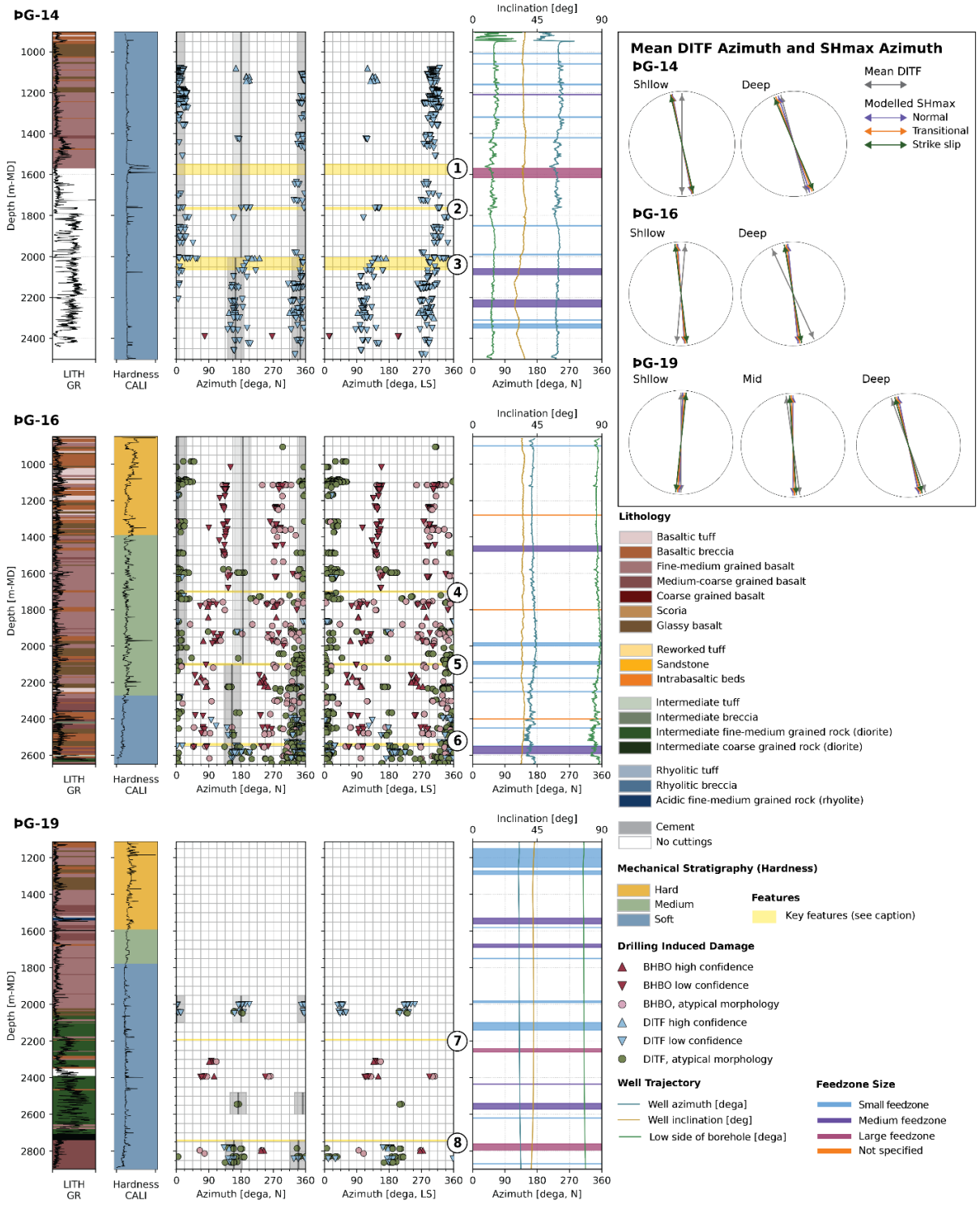


Figure 4: Results of our interpretation of drilling induced damage in ÞG-14, ÞG-16 and ÞG-19, with DITF and S_{Hmax} azimuth as indicated and contextual well data. Key features are: (1) a likely fault/fissure zone that is characterized by oversized borehole and wide fractures at 1550 – 1600 mMD; (2) scatter in the DITF azimuth at 1760 – 1770 mMD, likely due to the presence of a geologic discontinuity; (3) counter-clockwise rotation of DITF azimuth with a progressive change in azimuth from 2005 to 2065 mMD; (4) a change in the azimuthal spread and overall appearance of BHBO at 1700 mMD, likely due to a change in mechanical rock properties as indicated by the borehole rugosity (c.f., caliper); (5) rotation in mean DITF azimuth at 2100 mMD; (6) more scattered azimuths of atypical DITF below 2540 mMD, similar to what is observed around large feed zones in Indonesian, New Zealand and USA geothermal wells (Wallis et al., 2023b,c); and (7, 8) possible depth of stepwise stress rotation based on geologic context.

There are systematic relationships between the tendency results (T_s, T_d, and T_h) and fracture properties, specifically open vs closed fractures as defined by travel time and their width/aperture (Figure 5). As most clearly seen in the ÞG-16 case study, open fractures, especially those with larger apertures, tend to have a higher T_h than those that are closed. Wide fractures tend to have a higher T_d in ÞG-16. In all cases, wide fractures typically have higher T_s for a given T_d, more so as the relative magnitude of S_{Hmax} increases. ÞG-19 has a higher proportion of fractures with high T_h than ÞG-14 and ÞG-16, especially above the stress rotation at 2740 mMD.

We plotted fracture tendency with contextual geologic and reservoir engineering data to explore the relationship between our results and wellbore-scale fluid flux (Figure 6). Because fractures with high tendency occur throughout, there is no clear relationship between feed zone location and these results, with one clear exception. There is a cluster of fractures with wide apertures at 1547 – 1600 mMD in ÞG-14 that coincide with a large feed zone and have a range of T_s, high T_d, and high T_h (Feature 1, Figure 6). When projected to surface, these fractures correspond with a line of fumaroles mapped at surface. This cluster contrasts with one below ~2400 mMD in ÞG-14 that contains wide aperture fractures with low T_s, T_d, and T_h and no corresponding feed zone.

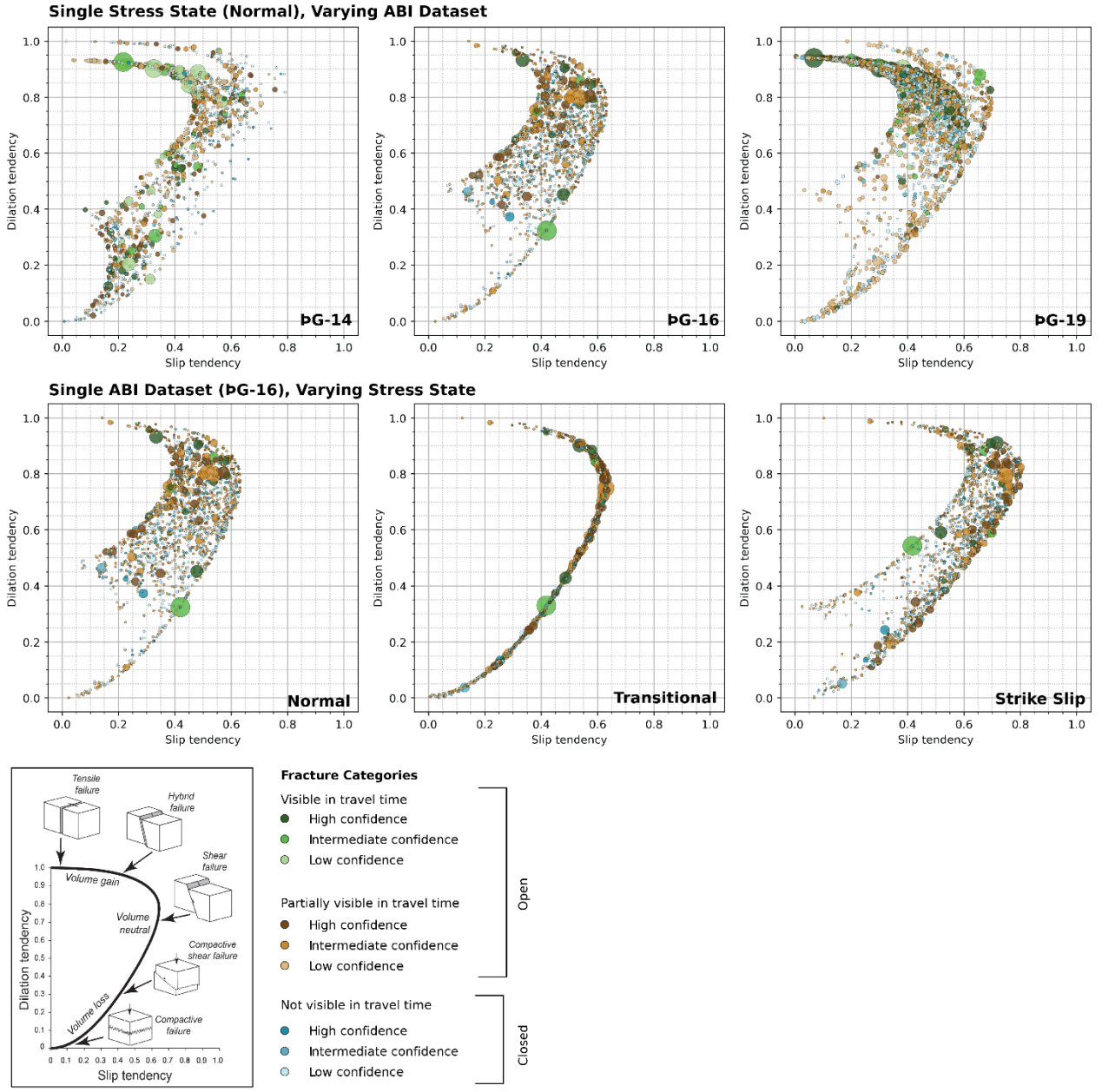


Figure 5: Sail plots that illustrate the variation of slip and dilatation tendency results by well and by stress state. Markers are colored by type classification and sized by aperture (for open fractures) or width (for closed fractures). Insert illustrating the expected failure mode for various sectors of the sail plot is from Ferrill et al. (2020).

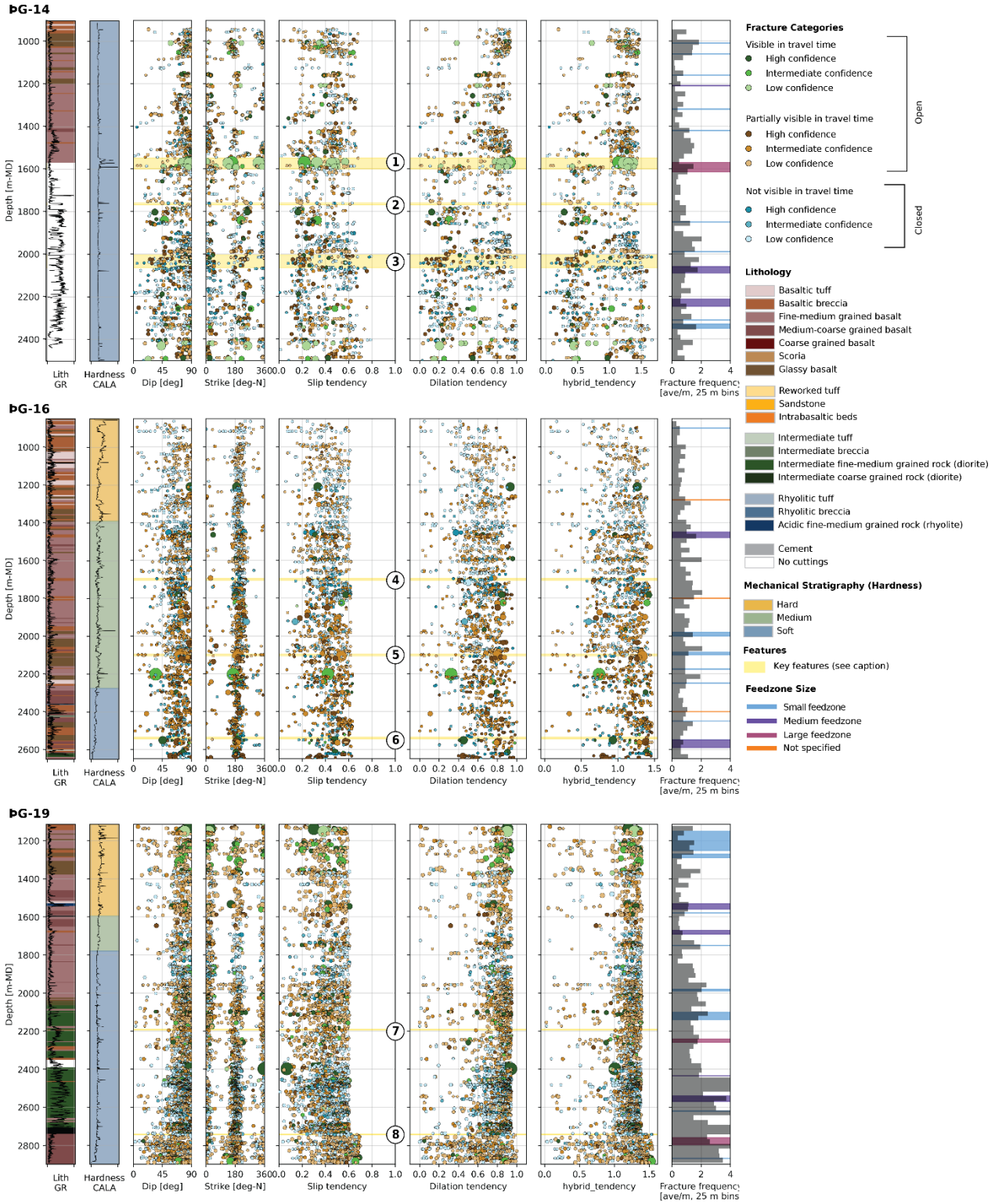


Figure 6: Slip and dilatation tendency results for the normal faulting case plotted by depth with contextual data. Key features are: (1) a likely fault/fissure zone that is characterized by oversized borehole and wide fractures at 1550 – 1600 mMD; (2) scatter in the DITF azimuth at 1760 – 1770 mMD, likely due to the presence of a geologic discontinuity; (3) counter-clockwise rotation of DITF azimuth with a progressive change in azimuth from 2005 to 2065 mMD; (4) a change in the azimuthal spread and overall appearance of BHBO at 1700 mMD, likely due to a change in mechanical rock properties as indicated by the borehole rugosity (c.f., caliper); (5) rotation in mean DITF azimuth at 2100 mMD; (6) more scattered azimuths of atypical DITF below 2540 mMD, similar to what is observed around large feed zones in Indonesian, New Zealand and USA geothermal wells (Wallis et al., 2023b,c); and (7, 8) possible depth of stepwise stress rotation based on geologic context.

3.3 Mechanical Stratigraphy

A simple mechanical stratigraphy was constructed using acoustic amplitude, lithology, and caliper data is plotted in Figures 4 and 6. The soft conditions are dominantly basaltic tuffs, breccia and glassy basalts (hyaloclastites). The hard conditions are dominantly basaltic and intermediate lavas. Average fracture frequency was lower in soft formation. This observation is unsurprising, given that stress may be accommodated by particle/clast rearrangement and/or ductile deformation in softer rocks. However, there is more borehole oversizing and surface roughness in the soft intervals. Therefore, the acoustic imager is less likely to resolve fractures. Wide, open fractures are less common in the soft intervals than in the hard, except for ~1115 – 1390 mMD in ÞG-19 where a group of wide, open fractures correspond to a thick but medium to large magnitude feed zone.

4 DISCUSSION

Our analysis of stress in three wellbore-scale case studies at Þeistareykir, and the slip (T_s), dilatation (T_d) and hybrid (T_h) tendency of fractures imaged therein, has generated insight into controls on permeability. In summary, we found abrupt rotations S_{Hmax} azimuth coincide with feed zones and reservoir-scale faults. T_s, T_d, and T_h results correspond to fracture aperture, but do not have a simple relationship to the distribution of feed zones. However, generally high T_h may generate a well-connected fracture network, favorable for production. Finally, mechanical rock properties are found to influence fracture frequency and relate to magnitude distribution of feed zones.

Our study revealed stepwise rotations of the S_{Hmax} azimuth in all three case studies. These rotations correspond to key structures identified at the reservoir-scale and feed zone locations. Our reservoir-scale dynamic stress modelling that used a simplified fault model for Þeistareykir also generated a counter-clockwise rotation in the S_{Hmax} azimuth (Siler et al, 2026, this volume), despite having specified a single average S_{Hmax} azimuth with depth in the natural state. This corroborates our conclusion that fault rupture is the likely cause of observed rotations in S_{Hmax} azimuth. Similar relationships between stress rotations, the presence of reservoir-scale faulting and the distribution of feed zones have been observed in silicic rift type volcanic-hosted geothermal systems in New Zealand (Wallis et al., 2020b; McNamara et al., 2015) and basement-hosted deep circulation geothermal systems in the western US (Fercho et al., 2020).

The T_s, T_d, and T_h results described herein resemble those that arose from outcrop studies by Ferrel et al. (2020) who mapped and modelled the ultra-low permeability Cretaceous Eagle Ford Formation and Austan Chalk, which are formations that host an unconventional oil and gas reservoir in south Texas, USA. Fault segments with high T_h were found to be more likely to form fluid flux conduits, with calcite vein cements (indicative of fluid flow) observed in fault segments with high T_d and low to moderate T_s (i.e. at the top of the sail plot). At Þeistareykir, open fractures, especially those with wider apertures, commonly have higher T_h than closed fractures. Wide fractures had clearly higher T_d than narrow fractures in one case, but they had higher T_s for a given T_d in all three cases (more so when the relative magnitude of S_{Hmax} increases). It would not have been possible to recognize these relationships without reliable identification of which fractures are open (at least at the wellbore wall) and a measurement of fracture width/aperture. This highlights the value of using acoustic borehole imagers, as the travel time data can be used to determine if a fracture is open at the borehole wall. While excess resistivity models have been used in cases to determine fracture aperture from microresistivity data (Luthi & Souhaite, 1990), this has been found to perform poorly in some cases (Wallis et al., 2024) and further validation work is required.

Because there are numerous fractures with high T_s, T_d, and T_h throughout the logged intervals, there is rarely a simple relationship between these parameters and the location or magnitude of feed zones. The exception is ÞG-14 where T_h may explain why one cluster of open fractures with wide apertures correspond to a large feed zone while another with similar fracture properties does not. A study of fracture T_s in four volcanic-hosted geothermal systems (silicic rift and arc type) similarly found that there was no simple correlation between fracture T_s and feed zones. This contrasts with the seminal work Barton et al. (1995) that demonstrated a relationship between high T_s (critically stressed fractures) and fracture-hosted fluid flow in three crustal wells that, based on their thermal gradient and geologic setting, were much lower permeability than is typical in conventional geothermal. These low-permeability conditions allowed Barton et al. (1995) to identify fluid hosting fractures through local inflections in a high-resolution temperature profile, something not possible in conventional geothermal given the well construction and in-wellbore dynamics.

The tendency modelling results herein indicate that ÞG-19 is more likely to form a connected fracture network than the other two cases because it has a greater proportion of fractures with high T_h than ÞG-14 and ÞG-16. ÞG-

19 is in the southwest of the well field and has high wellhead pressure and steam rate. While ÞG-14 to the north has the highest injectivity index of the case study wells, it is also the coolest and it contains fewer medium and large feed zones than ÞG-19. McLean (2020) conducted numerical pressure transient modelling of western wells ÞG-11, ÞG-15 and ÞG-17 (south-western wells that are close to ÞG-19) and an eastern well ÞG-16. They found that ÞG-16 matched a channel model with a restricted fracture network while the western wells fit a radial model that is more consistent with a well-connected fracture network. Future work includes further tendency modelling and integration with reservoir engineering analysis.

Using a simple, first-order mechanical stratigraphy, we found that average fracture frequency tends to be lower in soft formations. When all wells are considered together, we also found that larger feed zones are more common in hard formations (refer to Siler 2026, this issue). While this relationship between harder rock types and feed zone magnitude may relate to variation in fracture frequency, it is more likely to be a consequence of how asperities and/or fracture rugosity/sinuosity are more likely to prop open fractures in a hard rock and, therefore, sustain volume/aperture over time. While further work is needed to improve the mechanical stratigraphy, these results demonstrate that there is an underlying rock mechanical control on permeability at Þeistareykir.

5 CONCLUSIONS

Together with the companion paper Siler et al. (2026), the study described herein has demonstrated how our novel, multi-scale geomechanical workflow can reveal insight into the geologic controls on permeability in a complex, volcanic-hosted geothermal system. With a single exception, the three Þeistareykir wellbore-scale case studies found no simple relationship between the slip (T_s), dilatation (T_d) and hybrid (T_h) tendency of fractures and the location or magnitude of feed zones. This aligns with results from similar studies in silicic rift- and arc-type volcanic-hosted geothermal systems (Wallis, 2023). The location and magnitude of feed zones in volcanic-hosted geothermal systems are jointly influenced by the presence of active faulting (as indicated by stress rotations), favorable fracture characteristics (aperture, network connectivity, T_s, T_d, and T_h), and mechanical rock properties. On the surface, these findings appear to conflict with the now often cited control that critically stressed (high T_s) fractures have on fluid flux (Barton et al., 1995). However, this is more likely a matter of scale. Individual fracture T_s, T_d, and T_h characteristics influence the overall (background) permeability network and feed zones are wellbore-scale sweet spots with connection to the wider reservoir, resembling the numerical models of Hanano (2004). Given that feed zones require connection to the wider reservoir to sustain flow, it is important to place this wellbore-scale analysis within the context of the reservoir-scale distribution of permeability sweet spots—as is described in Siler et al. (2026). Through an improved understanding of the geologic mechanisms controlling permeability across scales, this workflow supports reservoir management strategies and future well targeting.

6 ACKNOWLEDGEMENTS

We would like to thank Landsvirkjun for supporting this study and granting permission to publish.

7 REFERENCES

Árnadóttir, S., Tryggvason, H.H., Gunnarsson, B.S., Pétursson, F., Gautason, B. & Blischke, A. (2018) Well ÞG-14. Results of Televiewer Imaging at the Þeistareykir Geothermal Field, NE-Iceland. Report prepared by Iceland GeoSurvey (ÍSOR) for Landsvirkjun.

Árnadóttir, S., Egilson, Þ., Níelsson, S., Pétursson, F., Hafsteinsson, H., & Jónsson, J.E. (2024) Well ÞG-19. Results of televiewer Imaging at the Þeistareykir geothermal field, NE-Iceland. Report prepared by Iceland GeoSurvey (ÍSOR) for Landsvirkjun.

Barton, C. A., Zoback, M. D., & Moos, D. (1995). Fluid flow along potentially active faults in crystalline rock. Geology, 23, 683–686.

Byerlee, J. (1978). Friction of rocks. Pure and Applied Geophysics, 116(4–5), 615–626.

Fercho, S., Hinz, N., Casteel, J., Turk, J., 2020. Analysis of Natural and Drilling Induced Fractures from Newly Acquired Borehole Image Logs at the Star Peak Geothermal Field, NV: Implications for Localized Stress Field Rotation Within a Normal Fault Step-Over. Geothermal Resources Council Transactions, 44.

Ferrill, D.A., Smart, K.J., and Morris, A.P., 2020. Resolved stress analysis, failure mode, and fault-controlled fluid conduits. Solid Earth, v11, p899-908. https://doi.org/10.5194/se-11-899-2020

Fractoolbox, https://github.com/ICWallis/fractoolbox. pre-alpha release, accessed 2025.

Foged, N.N. & Andreassen, K.A. (2016) Strengh and deformation properties of volcanic rocks in Iceland. Proceedings of the 17th Nordic Geotechnical Meeting, Reykjavik 25 – 28 May.

Hanano, M. (2004). Contribution of fractures to formation and production of geothermal resources. Renewable and Sustainable Energy Reviews, 8(3), 223–236.

Loftsson, M. & Steingrímsson, B.Ó. (2010) Petrotechnical properties of different rock types. Mannvit Open Report: 7-009-277.

McNamara, D. D., Massiot, C., Lewis, B., & Wallis, I. C. (2015). Heterogeneity of structure and stress in the Rotokawa Geothermal Field, New Zealand. Journal of Geophysical Research: Solid Earth, 120(2), 1243–1262.

McLean, P.K. (2020) Pressure Transient Analysis of Geothermal Wells: A Numerical Modelling Approach. University of Auckland Doctoral Thesis.

Luthi, S. M., & Souhaite, P. (1990). Fracture apertures from electrical borehole scans. Geophysics, 55(7), 821–833.

Peška, P., & Zoback, M. D. (1995). Compressive and tensile failure of inclined well bores and determination of in situ stress and rock strength. Journal of Geophysical Research: Solid Earth, 100(B7), 12791–12811.

Siler, D.L., 2023. Structural discontinuities and their control on hydrothermal systems in the Great Basin, USA. Geoenergy, 10 pp. https://doi.org/10.1144/geoenergy2023-009.

Siler, D.L., Wallis, I.C., Eggertsson, G.H., and Mortensen, A.K. (2026) Stress, Slip, and Productivity: Integrated Geomechanical Modeling of the Þeistareykir Geothermal Reservoir – Part 2 Reservoir-Scale. Proceedings World Geothermal Congress 2026, this volume.

Terzaghi, R. D. (1965). Sources of error in joint surveys. Geotechnique, 15(3), 287–304.

Þorsteinsdóttir, U., Árnadóttir, S., Gautason, B., Gunnarsson, B.S., Pétursson, F., Ingimarsson, H., & Egilson, Þ. (2018) Well ÞG-16. Results of Televiewer Imaging at the Þeistareykir Geothermal Field, NE-Iceland. Report prepared by Iceland GeoSurvey (ÍSOR) for Landsvirkjun.

Wallis, I., Pye, D.S., Dempsey, D., Rowland, J. (2020a) A users guide to leak-off test procedures and interpretation for geothermal wells. Proceedings of the World Geothermal Congress: Reykjavik, Iceland.

Wallis, I.C., Rowland, J. V., Dempsey, D. E., Allan, G., Sidik, R., Martikno, R., McLean, K., Sihotang, M., Azis, M. and Baroek, M. (2020b). Approaches to imaging feedzone diversity with case studies from Sumatra, Indonesia, and the Taupō Volcanic Zone, New Zealand. New Zealand Geothermal Workshop: Waitangi, New Zealand.

Wallis, I.C. (2023) The Geologic Controls on Geothermal Fluid Flux at the District-, Reservoir-, and Wellbore-Scale. University of Auckland Doctoral Thesis.

Wallis, I.C., Rowland, J.V., and Dempsey, D.E. (2023a) Geologic Controls on Geothermal System Location and Type. Transactions, New Zealand Geothermal Workshop.

Wallis, I.C., Dempsey, D.E., and Rowland, J.V. (2023b) Geologic Controls on Permeability Revealed by Borehole Imaging: Case Studies from Sumatra, Indonesia and the Taupō Volcanic Zone, New Zealand. Transactions, New Zealand Geothermal Workshop.

Wallis, I.C., Milton, A., Brown, Z., Davis, L., Casteel, J., and Peters, B., (2023c) Faults, Fractures, Formation, and Stress at Fish Lake: Controls on Wellbore-Scale Permeability in a Deep Circulation Geothermal System. GRC Transactions, Vol. 47.

Wallis, I.C., Wilson, A., Glass, F., and Bourdet, J. (2024) Borehole Image Log Analysis of Ramsay-1 and Ramsay-2 Part 2: Comparison of Aperture Analysis Methods Used to Constrain Secondary Porosity. Australian Natural Hydrogen Conference, 23 – 31 October, Adeliade Hills, Australia.

Wyering, L.D., Villeneuvea, M.C., Kennedy, B.M., Gravley, D.M., Siratovich, P.A. (2017) Using drilling and geological parameters to estimate rock strength in hydrothermally altered rock – A comparison of mechanical specific energy, R/N-W/D chart and Alteration Strength Index. Geothermics, 69. P 119-131.

Zoback, M. D. (2010). Reservoir Geomechanics. Cambridge University Press.